NANO LETTERS

Letter

pubs.acs.org/NanoLett

Mapping 3D Focal Intensity Exposes the Stable Trapping Positions of Single Nanoparticles

Anders Kyrsting, Poul M. Bendix, and Lene B. Oddershede*

Niels Bohr Institute, University of Copenhagen, Blegdamsvej 17, 2100, Denmark

Supporting Information

ABSTRACT: The photonic interactions between a focused Gaussian laser beam and a nanoscopic particle are highly dependent on exact particle location and focal intensity distribution. So far, the 3D focal intensity distribution and the preferred position of a nanoparticle confined within the focal region were only theoretically predicted. Here, we directly map the three-dimensional focal intensity distribution, quantify stable trapping positions, and prove that certain sizes of nanoparticles stably trap in front of the focus.

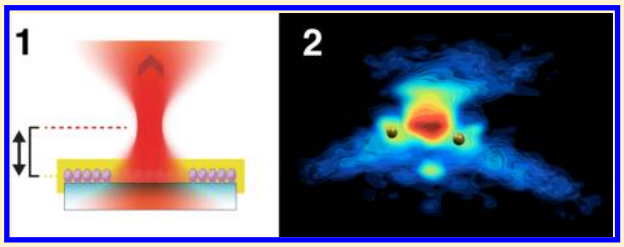

KEYWORDS: *Gold nanoparticles, nanoparticles, optical tweezers, focus intensity, surface plasmonics, spherical aberration*

The complex three-dimensional intensity distribution of a laser beam focused through a high numerical aperture objective has been theoretically addressed using vector theory.[1−3] These studies predict the existence of several local intensity maxima which are dependent on the possible presence of spherical aberration. Charge-coupled device (CCD) cameras have been employed to experimentally measure the intensity distribution within the focal region of a focused Gaussian laser beam.[4,5] However, this technique is limited by the spatial resolution of the CCD cameras. Slitted photodiodes can be used to measure the intensity but suffer from axial blurring due to the slit thickness and inherent polarizability sensitivity.[6] Mapping the intensity distribution in a diffraction limited laser spot with higher precision, and under different optical conditions, is important for improvements of the newly emerging super resolution optical microscopy techniques[7] overcoming the diffraction limit or in applications like fluorescence correlation spectroscopy. Measurements of intensity gradients near the focal region also provide information regarding the underlying optical trapping forces sensed by nanoscopic particles that, due to their tiny size, are particularly sensitive to local variations in the intensity distribution. The presence of metallic nanostructures[8] or the use of nonlinear effects of pulsed lasers[9] greatly enhances the local intensity gradients within the focal region.

The intensity gradient is responsible for the optical confinement of dielectric or metallic particles, where the most widespread optical configuration is simply a focused Gaussian laser beam, known as an optical trap.[10−12] For an optical trap based on a focused Gaussian laser beam it has been theoretically predicted that the scattering force would tend to push the equilibrium position of a trapped particle away from the exact focus of the objective in the direction of the propagating laser light.[13] This was measured for a micrometer-sized polystyrene particle[14] and assumed to hold true for metallic nanoparticles as well which have larger extinction cross sections.[15] Direct measurements of heating of metallic nanoparticles trapped in three dimensions proved that the larger metallic nanoparticles (over 100 nm in diameter) were significantly displaced from the most intense part of the laser focus; however, this assay gave no information regarding direction of the displacement.[16]

Here, we demonstrate a general method capable of mapping the intensity distribution within a laser spot focused at the focal plane of any type of light microscope. The assay used to measure the intensity distribution in the focal volume was based on bleaching of a thin layer of fluorophores adsorbed onto a coverslip which was moved in a controlled stepwise fashion through the focus (as sketched in Figure 1a and b). The fluorescent layer was Alexa555 labeled BSA (bovine serum albumin) evenly spread out over a glass coverslip in a 5−10 nm thick layer.[17] Sample chambers were open and consisted of a Teflon ring on top of a glass coverslip (No. 1 or No. 1.5, Menzel Gläser, Gerhard Menzel GmbH); the total volume of the sample chamber was ∼500 μL. The fluorescently labeled BSA layer was prepared by flushing 500 μL of a 0.5 mg/mL water solution of BSA-Alexa555 conjugate (A34786, Invitrogen) into the chamber and letting it incubate for 1 h at room temperature. Afterward, the chamber was thoroughly rinsed with Millipore water. The nanoparticles were sonicated for 30 min to remove possible aggregates and diluted 1000 times for the gold nanoparticles (BBIGold) and 1 million times for the fluorescent polystyrene spheres (F-8848, Invitrogen) before adding ∼5 μL of the bead solution to the sample chamber.

All images were acquired using a Leica SP5 confocal inverted microscope. An optical trap based on a 1064 nm laser (Spectra

Received: August 29, 2012
Revised: December 4, 2012
Published: December 10, 2012

dx.doi.org/10.1021/nl3032263 | *Nano Lett.* 2013, 13, 31−35

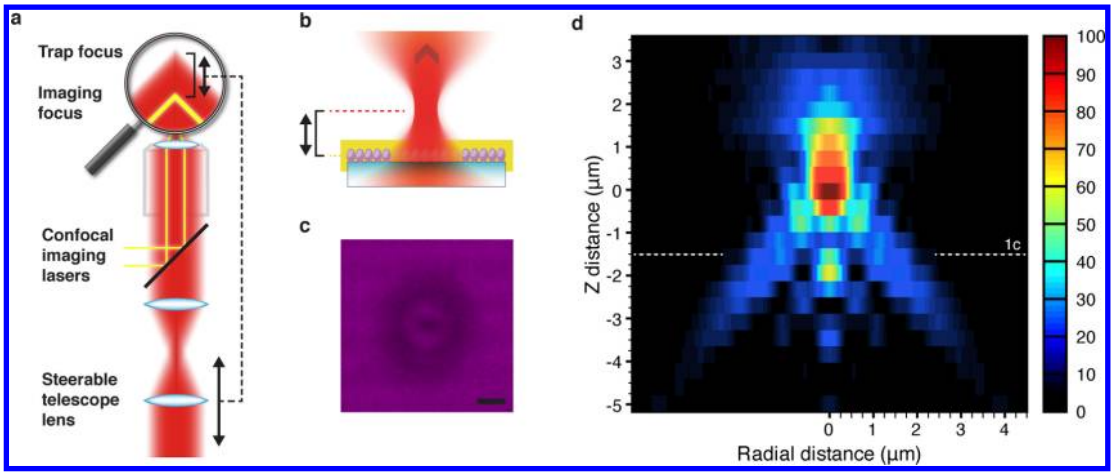

Figure 1. 3D mapping of the focal intensity distribution. (a,b) Sketches of the experiment where the NIR laser focus is moved in a stepwise fashion with respect to a fluorescently labeled BSA layer. This gives rise to a focal displacement between the focus of the NIR laser and the focus of the confocal imaging system; a shows the optics, b the sample region. (c) Raw image of the bleached BSA layer in a position corresponding to the situation shown in a and b; the scale bar is 1 μm. (d) Map of the NIR focal intensity for a 1.2 NA water immersion objective (cylindrical average). The white dashed line is the axial position corresponding to the image in c.

Physics J201-BL-106C operating in TEM_{00} CW mode) was implemented in the confocal microscope through a dichroic mirror in the Hg lamp housing.[18] Images were obtained by a point scanning laser, and the emitted light was collected using a photomultiplier tube and a confocal aperture of 1 airy unit. The BSA-Alexa555 layer was excited at 514 nm, and emitted light was collected at 529−705 nm. The gold particles were visualized using the backscattered light at 594 nm, and the yellow−green fluorescently labeled polystyrene spheres (F-8848, Invitrogen) were excited at 514 nm; emitted light was collected at 526−616 nm. The beads were imaged at different heights using different laser wavelengths to ensure that the obtained z positions were, within an uncertainty of ±20 nm, independent of imaging wavelength. To achieve maximum axial stability of the equipment, all lasers were switched on 30 min prior to the measurements. The z-position of the BSA layer was checked before and after a measurement, if drift had occurred the measurement was discarded. The two microscope objectives used were a 63× 1.2 NA Leica apochromatic water immersion objective (No. 11506279) and a 100× 1.4 NA Leica apochromatic oil objective (No. 11506210).

During an experiment the fluorophores within the focus of the 1064 nm laser were irradiated both by the 1064 nm laser and by the 514 nm confocal scanning laser. The bleaching rate of the fluorophore layer was determined by moving the stage at a constant lateral speed, while monitoring the bleaching. As shown in Supplementary Figure S1 the bleaching by the confocal laser alone was negligible in comparison to the combined effect of the two lasers. Hence, the bleached fingerprint (as shown in Figure 1c) of the fluorophores on the glass surface is a negative image of the intensity in the 1064 nm laser focus. The linear relation between the 1064 nm laser power and the bleaching rate probably is a result of a sequential absorption of a 514 nm and a 1064 nm photon as previously reported.[19] This linear relation allowed for a direct conversion from the reduction in the fluorescence signal to intensity of the near-infrared (NIR) laser at the same location. In the experiment, the sample was moved in the lateral direction to a fresh and unbleached part of the flourescent layer, and a scanning confocal image containing the fingerprint of the 1064 nm focus was acquired (while both lasers were turned on simultaneously). Subsequently, the axial position of the focus of the trapping laser was moved with respect to the focus of the confocal microscope. This was done by moving the position of the first telescope lens (see schematic diagram of the setup in Figure 1a) while keeping the objective and sample fixed in the axial direction. Immediately before acquiring a scanning confocal image, the fluorescent layer was again translated in the lateral direction to reveal a fresh and nonbleached part of the fluorescent layer.

The slices acquired at the plane of the fluorescent BSA layer by linearly stepping the laser focus through the focus of the confocal imaging were gathered to obtain a 3D image of the intensity distribution of the focused NIR laser, as shown in Figure 1d. To create this image, the raw images were inverted (highest degree of bleaching is shown in red, lowest in black), filtered to remove periodic line noise, deconvoluted by the 514 nm confocal point spread function using a total variation regularization Lucy-Richardson[20] algorithm, and averaged cylindrically around the beam axis. A cylindrical average was justified by the fact that the intensity profile was nearly cylindrically symmetric, and the full 3D intensity profile (without cylindrical averaging) is shown in Supplementary Videos 1 and 2.

The lateral distances were read off directly from the confocal imaging. To get the absolute values in the axial direction we compared the axial intensity distribution from a AuNP measured by two methods: (i) The particle was attached to the surface and imaged by normal confocal z-stacking; this yielded the axial intensity distribution in units of nanometers. (ii) The particle was held in solution by the optical trap, and the axial position of the trap was moved with respect to the (constant) plane of confocal scanning by the telescope lens, thus yielding the axial intensity distribution in arbitrary units. By equating the standard deviations of the axial intensity distributions obtained by methods (i) and (ii) (shown in Supplementary Figure S2), we obtained a calibration factor converting the arbitrary units of method (ii) to nanometers. The obtained intensity profile (as shown in Figure 1d) is in accordance with previous experimental mappings;[5,6] however, significantly more features, especially in the axial direction, are here resolved. In comparison to literature, the axial resolution is

dx.doi.org/10.1021/nl3032263 | Nano Lett. 2013, 13, 31−35

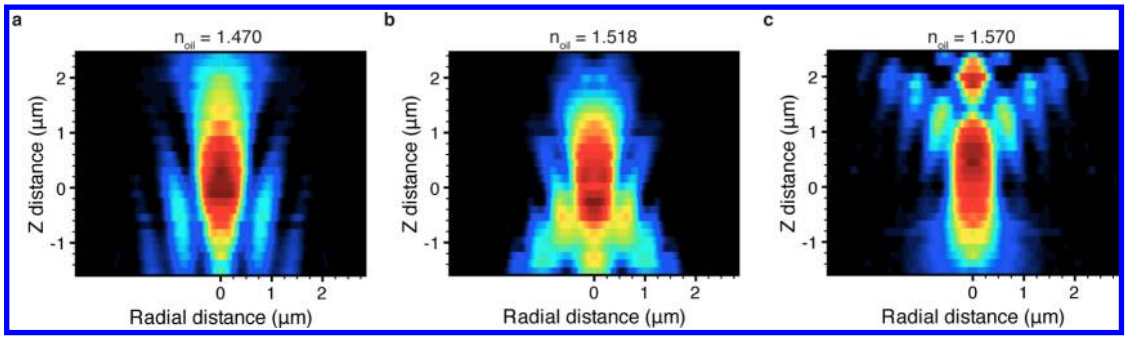

Figure 2. Spherical aberration affects the focal intensity distribution. Mappings of focal intensity just above the coverslip surface while focusing the laser light by an 1.4 NA oil immersion objective using immersion media with different refractive indices, *n*. (a) n_{oil} = 1.470 causes aberration toward the objective. (b) n_{oil} = 1.518 creates a nearly ideal and strong focus. (c) n_{oil} = 1.570 creates aberration pointing away from the objective.

here significantly improved since no out of focus light entered the focus when imaging the fluorescent 2D BSA layer. The axial precision is determined by the thickness of the fluorescent layer and the axial stability of the microscope. In the current experiments we estimate our axial resolution to be ~50 nm. It is clear from Figure 1d that the infrared laser light underwent significant spherical aberration while focused by a water immersion objective optimized for visible wavelengths.[21] Also, the experimentally measured intensity distribution is in accordance with theoretical predictions.[1,3,22]

To further investigate the intensity distribution in foci affected by different degrees of spherical aberration, we repeated the experiment using a 100× 1.4 NA oil immersion objective. By changing the index of refraction of the immersion media, n_{oil}, additional spherical aberration was introduced in a controlled fashion.[23] By using an immersion media with n_{oil} = 1.470, 1.518, and 1.570, respectively, we got mappings of the focal intensity close to the coverslip in the presence of spherical aberration as seen in Figure 2. As expected,[22,23] n_{oil} = 1.518 provides the strongest and least aberrated focus close to the surface, whereas n_{oil} = 1.470 and n_{oil} = 1.570 causes the focus to be more aberrated and in opposite axial directions.

It has long been an outstanding question in the optical trapping community exactly where in the focal region trapped particles are located. The general consensus has been that particles, both microscopic polystyrene particles[13] and nanoscopic metallic nanoparticles[15] were pushed in the direction of the propagating laser light due to the scattering force. To map out the nanoscale potential landscape of the NIR focus, we optically trapped nanoparticles in the focal region and imaged their locations by collecting the back-scattered light using an acousto optical beam splitter.[11,12,16] To avoid interactions with the surface, the particles were trapped ~10 μm into the sample. For these experiments, we used the water immersion objective as no additional aberration was introduced as the focus was translated in the axial direction.

While translating the trapping focus through the confocal focus, we collected the 594 nm laser light scattered off from the trapped particle, images of an 80 nm AuNP at various distances are shown in Figure 3a. The scattered intensity was highest when the focus of the confocal imaging system coincided with the position of the trapped particle (around z = 298 nm in Figure 3a). The axial position of the trapped particle with respect to the focus of the NIR laser was then determined as the maximum of a Gaussian function fitted to the intensity distribution (as shown in Figure 3b). This yielded an axial precision of ~50 nm on the position determination of particles

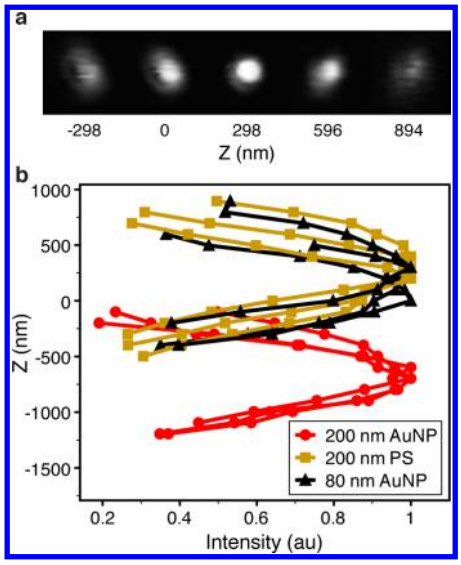

Figure 3. Axial position of a trapped particle with respect to NIR laser focus. (a) Image series showing the intensity of 594 nm laser light scattered off from an optically trapped 80 nm gold nanoparticle collected at various heights. (b) Intensity of scattered light as function of distance from NIR focus for trapped 80 nm AuNPs (black), 200 nm AuNPs (red), and 200 nm polystyrene particles (yellow, for these the fluorescently emitted light was detected).

diffusing in the optical trap. To test our method, we determined the axial center position of AuNPs attached to a glass coverslip subsequently covered by a fluorescent BSA layer. We found the distances between the beads' centers and the BSA layer to be 67 ± 36 nm and 5 ± 28 nm for 200 and 80 nm AuNPs, respectively (data is shown in Supplementary Figure S3a,b). Adding the thickness of the BSA layer, ~10 nm, the numbers are in accordance with the expected radii of the particles. For the method to be valid, it is also important that the light scattered from a trapped particle is independent of trapping depth, as is indeed the case for trapping deeper than ~4 μm into the sample (Supplementary Figure S4).

The axial position of the particle and the intensity distribution within the focal region were overlaid to locate the particle relative to the focal intensity distribution (Figure 4). The lateral trapping positions were found by overlaying the confocal images of the bleached BSA layers with the images of the light scattered off the trapped particles; examples are shown in Figure 4b, c, and d for a 200 nm polystyrene particle, an 80 nm AuNP, and a 200 nm AuNP, respectively. Similarly, the axial positions of the trapped particles, measured in Figure 3,

dx.doi.org/10.1021/nl3032263 | *Nano Lett.* 2013, 13, 31−35

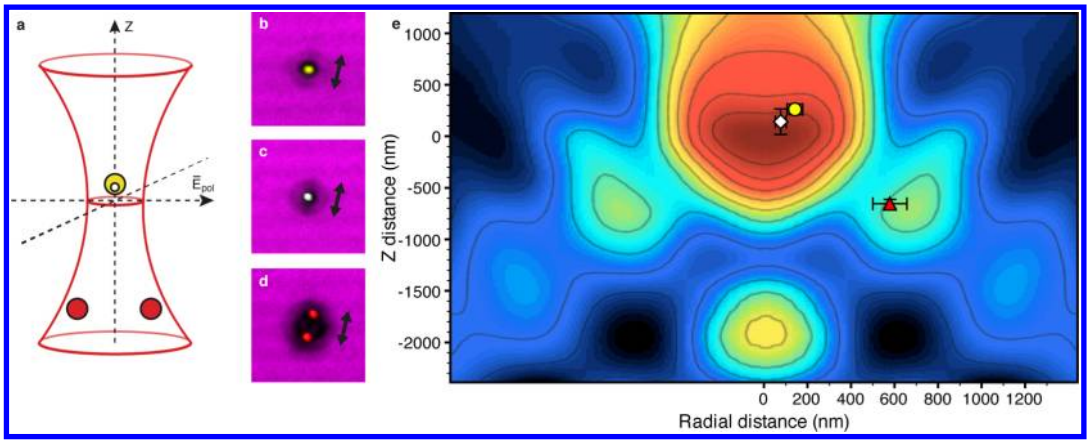

Figure 4. Nanoparticle trapping positions within the focal region. (a) Illustration of the most likely trapping positions within the focal region (yellow sphere: 200 nm polystyrene, white sphere: 80 nm AuNPs, red spheres: 200 nm AuNPs). (b, c, d) Overlay of bleached fluorescently labeled BSA layer and confocal recording of the scattered or fluorescent light from from a 200 nm polystyrene particle, an 80 nm AuNP, and from two 200 nm AuNPs, respectively. Arrows show the direction of the laser polarization vector and serve as scale bars (1.5 μm). (e) Overlay of axially smoothed version of Figure 1d with an average of trapped particle positions (same color code as Figure 1d); error bars denote one standard deviation obtained from measured positions of ~7 particles. We note that this is a cylindrical average; hence the right part is a mirror of the left part and the radial distance as well as nanoparticle positions are only given on the right half. The full 3D intensity map (without cylindrical averaging) is given in Supplementary Videos 1 and 2. All data were obtained using a laser power of 315 mW at the focus.

were overlaid with the intensity distribution, measured in Figure 1d, by correlating the telescope lens settings in the two experiments. As expected,[13] 200 nm polystyrene particles and 80 nm AuNPs were trapped just above the most intense part of the focal region (data shown in Figure 4e). Interestingly, and in contrast to our expectations, the 200 nm AuNPs were stably trapped off axis and in front of the laser focus in local intensity maxima.

Supplementary Figure S5 shows that the bleached area, hence, the lateral intensity distribution, is elongated along the direction of the polarization vector as previously observed.[6] Accordingly, the 200 nm AuNPs occupied multiple stable trapping positions in the lateral direction along the direction of the laser polarization vector (shown with arrows in Figure 4b, c, d, and the particle positions are shown in Supplementary Video 3). We found that the 200 nm AuNPs trap at local intensity maxima laterally displaced 600 nm away from the beam axis and approximately 650 nm below the point of maximum intensity in the axial direction. Also the polystyrene particles are slightly, but significantly, displaced from focus center in the lateral direction. Supplementary Videos 1 and 2 provide 3D visualizations of the exact trapping positions of gold and polystyrene nanoparticles through an unpeeling of the intensity distributions in the lateral and axial directions, respectively. The local intensity maxima are surrounded by local intensity gradients responsible for particle confinement. The gold particle manufacturer states a size dispersion of ~10%, which could explain the spread in stable trapping positions which is larger than the estimated position detection error (~50 nm in the axial direction, ~10 nm in the lateral direction).

To stably trap 200 nm AuNPs for a time long enough to translate them through the confocal scanning plane, a 1064 nm laser power of at least 315 mW had to be applied. At all laser laser power, P, of at least 315 mW had to be applied. At all laser powers (315 mW < P < 1000 mW) the 200 nm AuNPs appeared to be located below the focus, never at or above the focus. The fact that 200 nm AuNPs cannot be trapped at the center of the trap is consistent with calculations showing that the heating of 200 nm AuNPs, placed at the center of the laser focus, reaches temperatures exceeding the critical temperature of water (T = 647 K) even at the power of P = 315 mW.

The focal intensity maps here presented were obtained without a particle in the focus. Irradiation of a metallic nanoparticle changes the near-field of the particle;[24] hence, it is expected that the focus intensity adjacent to the particle will change when the particle is present. The expected spatial range of the near-field extending from the particle is on the order of tens of nanometers,[24] and hence, it would not be detectable with a method relying on confocal microscopy. Future investigations refining the methods presented in the current paper might be able to resolve such particle-induced near-field enhancements.

We presented a direct, novel measurement of the three-dimensional intensity distribution within a laser focus with high axial resolution. This 3D mapping can be readily applied in systems which combine confocal microscopy with optical micromanipulation often used in biophysical studies where force is applied during imaging.[25] Also, this method of using a short wavelength point scanning laser to map out the intensity distribution of a longer wavelength stationary laser focus is relevant for the development of new optical techniques trying to break the optical diffraction limit by combining two lasers.[7,26] A controlled introduction of spherical aberration, by changing the index of refraction of the immersion media,[23] accordingly changed the intensity distribution within the focal region. Mapping the focal intensity exposed the stable trapping positions of nanoparticles. Whereas 80 nm AuNPs and 200 nm polystyrene particles were stably trapped at the expected location slightly above the focus, the observed stable trapping position of 200 nm AuNPs in front of the focus was highly unexpected. Also, we note the striking similarity between the two stable lateral trapping postions of 200 nm AuNPs here observed and the recently reported splitting of a trap[9] which was attributed to a nonlinear optical effect. A detailed mapping of the focal intensity and a correct understanding of the position of an irradiated metallic nanoparticle within the focus is highly important for understanding and utilizing photonic interactions between nanoscopic particles and focused electro-

dx.doi.org/10.1021/nl3032263 | *Nano Lett.* 2013, 13, 31−35

magnetic fields, these interactions becoming increasingly relevant in nanophotonic applications like nanosensing,[27] locating nanoparticle trapping positions,[28] or photothermal therapy.

■ ASSOCIATED CONTENT

Supporting Information

Supplementary Figure 1: BSA bleaching rate for confocal 514 nm laser and trapping 1064 nm laser. Supplementary Figure 2: Axial intensity distribution determined by confocal microscopy. Supplementary Figure 3: Distance between the center of the surface attached AuNPs and the BSA layer. Supplementary Figure 4: Backscattered signal from individual AuNPs trapped at various depths within the sample. Supplementary Figure 5: Elongation of the lateral intensity distribution along the 1064 laser polarization vector. Video 1: Intensity profile, lateral peel. Video 2: Intensity profile, axial peel. Video 3: Occupancy of multiple stable trapping positions for 200 nm AuNPs. This material is available free of charge via the Internet at http://pubs.acs.org.

■ AUTHOR INFORMATION

Corresponding Author

*E-mail: oddershede@nbi.dk.

Notes

The authors declare no competing financial interest.

■ ACKNOWLEDGMENTS

This work was supported by the Lundbeck Foundation, the Carlsberg Foundation, and the Excellence Program at University of Copenhagen.

■ REFERENCES

(1) Li, Y.; Yu, F. T. S. *Opt. Commun.* **1989**, *70*, 1−7.
(2) Li, Y.; Wolf, E. *J. Opt. Soc. Am. A* **1982**, *1*, 801−808.
(3) Nasse, M. J.; Woehl, J. C. *J. Opt. Soc. Am. A* **2010**, *27*, 295−302.
(4) Karman, G. P.; Van Duijl, A.; Beijersbergen, M. W.; Woerdman, J. P. *Appl. Opt.* **1997**, *36*, 8091−8095.
(5) Schneider, M. B.; Webb, W. W. *Appl. Opt.* **1981**, *20*, 1382−1388.
(6) Dorn, R.; Quabis, S.; Leuchs, G. *J. Mod. Opt.* **2003**, *50*, 1917−1926.
(7) Hell, S. W.; Schmidt, R.; Egner, A. *Nat. Photonics* **2009**, *3*, 381−387.
(8) Chen, J.; Ng, J.; Lin, Z.; Chan, C. T. *Nat. Photonics* **2011**, *5*, 531−534.
(9) Jiang, Y.; Narushima, T.; Okamoto, H. *Nat. Phys.* **2010**, *6*, 1005−1009.
(10) Ashkin, A.; Dziedzic, J. M.; Bjorkholm, J. E.; Chu, S. *Opt. Lett.* **1986**, *11*, 288−290.
(11) Svoboda, K.; Block, S. M. *Opt. Lett.* **1994**, *19*, 930−932.
(12) Hansen, P. M.; Bhatia, V. K.; Harrit, N.; Oddershede, L. B. *Nano Lett.* **2005**, *5*, 1937−1942.
(13) Rohrbach, A.; Stelzer, E. H. K. *J. Opt. Soc. Am. A* **2001**, *18*, 839−853.
(14) Neuman, K. C.; Block, S. M. *Rev. Sci. Instrum.* **2004**, *75*, 2787−2809.
(15) Seol, Y.; Carpenter, A. E.; Perkins, T. T. *Opt. Lett.* **2006**, *31*, 2429−2431.
(16) Kyrsting, A.; Bendix, P. M.; Stamou, D. G.; Oddershede, L. B. *Nano Lett.* **2011**, *11*, 888−892.
(17) Su, T. J.; Lu, J. R.; Thomas, R. K.; Cui, Z. F. *J. Phys. Chem. B* **1999**, *103*, 3727−3736.
(18) Richardson, A. C.; Reihani, N.; Oddershede, L. B. *Proc. SPIE* **2006**, *6326*, 632628.
(19) van Dijk, M. A.; Kapitein, L. C.; van Mameren, J.; Schmidt, C. F.; Peterman, E. J. G. *J. Phys. Chem. B* **2004**, *108*, 6479−6484.
(20) Dey, N.; Blanc-Feraud, L.; Zimmer, C.; Roux, P.; Kam, Z.; Olivo-Marin, J.; Zerubia, J. *Microsc. Res. Techn.* **2006**, *69*, 260−266.
(21) Reihani, S. N. S.; Mir, S. A.; Richardson, A. C.; Oddershede, L. B. *J. Opt.* **2011**, *13*, 105301.
(22) Rohrbach, A.; Stelzer, E. H. K. *Appl. Opt.* **2002**, *41*, 2494−2507.
(23) Reihani, S. N. S.; Oddershede, L. B. *Opt. Lett.* **2007**, *32*, 1998−2000.
(24) Plech, A.; Kotaidis, V.; Lorenc, M.; Boneberg, J. *Nat. Phys.* **2006**, *2*, 44−47.
(25) Sorre, B.; Callan-Jones, A.; Manneville, J.-B.; Nassoy, P.; Joanny, J.-F.; Prost, J.; Goud, B.; Bassereau, P. *Proc. Natl. Acad. Sci.* **2009**, *106*, 5622−5626.
(26) Rittweger, E.; Han, K. Y.; Irvine, S. E.; Eggeling, C.; Hell, S. W. *Nat. Photonics* **2009**, *3*, 144−147.
(27) Ohlinger, A.; Deak, A.; Lutich, A. A.; Feldmann, J. *Phys. Rev. Lett.* **2012**, *108*, 018101.
(28) Balijepalli, A.; Gorman, J. J.; Gupta, S. K.; LeBrun, T. W. *Nano Lett.* **2012**, *12*, 2347−2351.